J|A|C|S ARTICLES

Published on Web 09/21/2010

Planar to Linear Structural Transition in Small Boron−Carbon Mixed Clusters: $C_xB_{5-x}^-$ ($x = 1-5$)

Lei-Ming Wang,[†] Boris B. Averkiev,[‡] Jordan A. Ramilowski,[‡] Wei Huang,[†] Lai-Sheng Wang,*[,†] and Alexander I. Boldyrev*[,‡]

Department of Chemistry, Brown University, Providence, Rhode Island 02912, and Department of Chemistry and Biochemistry, Utah State University, Logan, Utah 84322

Received May 5, 2010; E-mail: Lai-Sheng_Wang@brown.edu; a.i.boldyrev@usu.edu

Abstract: Bulk carbon and boron form very different materials, which are also reflected in their clusters. Small carbon clusters form linear structures, whereas boron clusters are planar. For example, it is known that the B_5^- cluster possesses a C_{2v} planar structure and C_5^- is a linear chain. Here we study B/C mixed clusters containing five atoms, $C_xB_{5-x}^-$ ($x = 1-5$), which are expected to exhibit a planar to linear structural transition as a function of the C content. The $C_xB_{5-x}^-$ ($x = 1-5$) clusters were produced and studied by photoelectron spectroscopy; their geometric and electronic structures were investigated using a variety of theoretical methods. We found that the planar-to-linear transition occurs between $x = 2$ and 3: the global minimum structures of the B-rich clusters, CB_4^- and $C_2B_3^-$, are planar, similar to B_5^-, and those of the C-rich clusters, $C_3B_2^-$ and C_4B^-, are linear, similar to C_5^-.

1. Introduction

Boron and carbon are among the most refractory materials owing to their strong chemical bonding capacities. Boron carbides are also highly refractory materials with a range of stoichiometry. However, compared to bare boron and carbon clusters, boron−carbon mixed clusters have received relatively little experimental attention. Small carbon clusters (up to C_9) are known to possess linear structures,[1] while small boron clusters with less than 20 atoms have been shown to be planar or quasi-planar.[2] Among the experimentally characterized boron/carbon mixed clusters, C_2B, C_3B, and C_2B_2 have been established to be linear from infrared spectroscopy.[3,4] C_nB^- cluster anions with $n < 13$ were generated from laser vaporization and studied by mass spectrometry and ab initio calculations, showing that C_nB^- with even n are much more stable than those with odd n.[5] Large boron-doped carbon clusters of the type B_mC_n ($m = 1-4$, $2 \le n \le 400$) have also been produced by the laser vaporization cluster beam technique.[6]

The CB_6^{2-}, CB_7^-, and CB_8 clusters have been theoretically proposed to be hexa-, hepta-, and octacoordinated planar carbon species, respectively.[7−9] However, our recent joint experimental and theoretical investigations have shown that the hypercoordinate D_{6h} CB_6^{2-}, D_{7h} CB_7^-, and D_{8h} CB_8 clusters are highly unstable:[10−12] carbon seems to avoid the central position and hypercoordination in these species. Pei and Zeng[13] computed the planar tetra-, penta-, hexa-, hepta-, and octacoordinated structures in boron−carbon mixed clusters and again found that in all the species tested carbon avoids hypercoordination. Theoretical calculations of other carbon−boron clusters have been reported, showing that linear or planar structures are among the most stable ones when the number of atoms is relatively small.[14−24]

[†] Brown University.
[‡] Utah State University.

(1) Van Orden, A.; Saykally, R. J. *Chem. Rev.* **1998**, *98*, 2313.
(2) (a) Zhai, H. J.; Wang, L. S.; Alexandrova, A. N.; Boldyrev, A. I. *J. Chem. Phys.* **2002**, *117*, 7917. (b) Alexandrova, A. N.; Boldyrev, A. I.; Zhai, H. J.; Wang, L. S. *Coord. Chem. Rev.* **2006**, *250*, 2811. (c) Zubarev, D. Y.; Boldyrev, A. I. *J. Comput. Chem.* **2007**, *28*, 251.
(3) Presilla-Marquez, J. D.; Larson, C. W.; Carrick, P. G. *J. Chem. Phys.* **1996**, *105*, 3398.
(4) Presilla-Marquez, J. D.; Carrick, P. G.; Larson, C. W.; Rittby, C. M. L. *J. Chem. Phys.* **1999**, *110*, 5702.
(5) Wang, C. R.; Huang, R. B.; Liu, Z. Y.; Zheng, L. S. *Chem. Phys. Lett.* **1995**, *242*, 355.
(6) Kimura, T.; Sugai, T.; Shinohara, H. *Chem. Phys. Lett.* **1996**, *256*, 269.
(7) Exner, K.; Schleyer, P. v. R. *Science* **2000**, *290*, 1937.
(8) Wang, Z.-X.; Schleyer, P. v. R. *Science* **2001**, *292*, 2465.
(9) Minyaev, R. M.; Gribanova, T. N.; Starikov, A. G.; Minkin, V. I. *Mendeleev Commun.* **2001**, *11*, 213.
(10) Averkiev, B. B.; Zubarev, D. Yu.; Wang, L. M.; Huang, W.; Wang, L. S.; Boldyrev, A. I. *J. Am. Chem. Soc.* **2008**, *130*, 9248.
(11) Wang, L. M.; Huang, W.; Averkiev, B. B.; Boldyrev, A. I.; Wang, L. S. *Angew. Chem., Int. Ed.* **2007**, *46*, 4550.
(12) Averkiev, B. B.; Wang, L. M.; Huang, W.; Wang, L. S.; Boldyrev, A. I. *Phys. Chem. Chem. Phys.* **2009**, *11*, 9840.
(13) Pei, Y.; Zeng, X. C. *J. Am. Chem. Soc.* **2008**, *130*, 2580.
(14) Martin, J. M. L.; Taylor, P. R. *J. Chem. Phys.* **1994**, *100*, 9002.
(15) Zhan, C. G.; Iwata, S. *J. Phys. Chem. A* **1997**, *101*, 591.
(16) Wang, L. J.; Zhang, C. J.; Wu, H. S. *Acta Phys.-Chim. Sin.* **2005**, *21*, 244.
(17) Chuchev, K.; BelBruno, J. J. *J. Phys. Chem. A* **2004**, *108*, 5226.
(18) Ge, M. F.; Feng, J. K.; Huang, X. R.; Yang, C.; Sun, J. Z. *Chem. J. Chin. U.* **1997**, *17*, 1458.
(19) Ge, M. F.; Huang, X. R.; Feng, J. K.; Yang, C.; Sun, J. Z. *Chem. J. Chin. U.* **1997**, *18*, 1838.
(20) Zhang, J. L.; Wang, L. B.; Wu, W. P.; Cao, Z. X. *Acta Chim. Sin.* **2005**, *63*, 131.
(21) Wang, L. J.; Zhang, C. J. *Acta Phys.-Chim. Sin.* **2006**, *22*, 726.
(22) McAnoy, A. M.; Bowie, J. H.; Blanksby, S. J. *J. Phys. Chem. A* **2003**, *107*, 10149.
(23) (a) Liu, C. H.; Tang, M. S.; Wang, H. M. *J. Phys. Chem. A* **2007**, *111*, 704. (b) Wang, R.; Zhang, D.; Zhu, R.; Liu, C. *J. Mol. Struct.: THEOCHEM* **2007**, *817*, 119.
(24) Shao, J.; Zhu, X.; Lu, X.; Shi, R. *J. Mol. Struct.: THEOCHEM* **2008**, *855*, 82.

 10.1021/ja103846q

The boron pentamer B_5^- is known to possess a "W"-shaped planar structure,[25] while C_5^- is linear with a $^2\Pi_u$ ground electronic state.[1] In the current article, we report a joint photoelectron spectroscopy and ab initio investigation on the five-atom carbon−boron mixed clusters $C_xB_{5-x}^-$ ($x = 1-5$), revealing a planar-to-linear structural transition upon increasing the number of carbon atoms in this series. It is found that CB_4^- and $C_2B_3^-$ display similar "W"-shaped planar structures as B_5^-, while $C_3B_2^-$ and C_4B^- possess linear structures similar to C_5^-.

2. Experimental Methods

The experiment was performed using a magnetic-bottle PES apparatus equipped with a laser vaporization cluster source, details of which have been published elsewhere.[26] Briefly, the $C_xB_{5-x}^-$ clusters were produced by laser vaporization of composite targets made with isotopically enriched ^{10}B and different percentages of C to optimize the cluster abundance: ~5% C for CB_4^-, $C_2B_3^-$, and $C_3B_2^-$ or ~8% C for C_4B^- and C_5^-. A helium carrier gas was used at a backing pressure of 10 atm delivered by a pair of Jordan pulsed valves (Jordan Inc., CA).[26] A 10-cm long, 3-mm diameter stainless tube was used as an extension to the source nozzle to allow adequate thermalization and cooling of the nascent clusters.[11] Negatively charged clusters were extracted from the cluster beam and analyzed using a time-of-flight mass spectrometer. The $C_xB_{5-x}^-$ ($x = 1-5$) clusters of interest were mass selected and decelerated before being intercepted by a 193 nm (6.424 eV) laser beam from an ArF excimer laser or 355 nm (3.496 eV) and 266 nm (4.661 eV) from a Nd:YAG laser for photodetachment. Photoelectron time-of-flight spectra were measured and calibrated using the known spectra of Au^- at 193 nm or Rh^- at 266 and 355 nm and converted to the binding energy spectra by subtracting the kinetic energy spectra from the corresponding photon energies. The energy resolution of the magnetic-bottle PES spectrometer is $\Delta E/E \approx 2.5\%$, i.e., about 25 meV for 1 eV electrons.

3. Theoretical Methods

Computationally we first searched for the global minimum of $C_xB_{5-x}^-$ ($x = 1-5$) using the B3LYP/6-311+G* level of theory.[27−31] The geometries of the global minimum structures and some low-lying isomers were then recalculated at higher levels of theory using U(R)CCSD(T)/6-311+G* and U(R)CCSD(T)/aug-cc-DZ.[32−35]

To compare with the experimental results, the vertical electron detachment energies (VDEs) of $C_xB_{5-x}^-$ ($x = 1-5$) were calculated using the RCCSD(T)/6-311+G(2df) method, the outer valence Green Function method [ROVGF/6-311+G(2df)][36−38] at the RCCSD(T)/6-311+G* geometries, and the time-dependent DFT method [(TD-B3LYP/6-311+G(2df)][39,40] at the optimized B3LYP/6-311+G* geometries. In the last approach, the first VDE was calculated at the B3LYP level of theory as the lowest transition from the anion into the neutral clusters. Then the vertical excitation energies of the neutral species (at the TD-B3LYP level) were added to the first VDE to obtain the second and higher VDEs. Core electrons were frozen in treating the electron correlation at the RCCSD(T) and ROVGF levels of theory. The B3LYP, RCCSD(T), ROVGF, and TD-B3LYP calculations were performed using the Gaussian 03 and Molpro programs.[41,42] Molecular structure visualization was done using the MOLDEN 3.4 program.[43]

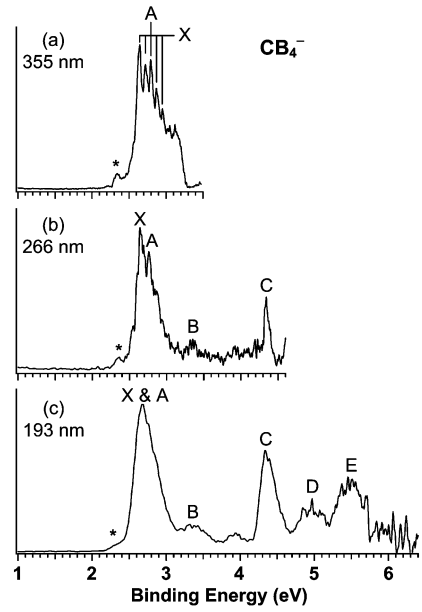

Figure 1. Photoelectron spectra of CB_4^- at (a) 355 nm (3.496 eV), (b) 266 nm (4.661 eV), and (c) 193 nm (6.424 eV).

4. Experimental Results

4.1. Photoelectron Spectra of CB_4^-. The photoelectron spectra of CB_4^- at three photon energies are shown in Figure 1. At 355 nm (Figure 1a), a series of sharp peaks is observed with roughly equal spacings, indicating that they are from one vibrational progression. However, the relative intensity of the third peak (A) is apparently too high, deviating from a single Franck−Condon profile. This observation suggests that there may be another electronic detachment transition overlapping with the ground state vibrational progression. The first intense vibrational peak of the X band defines an ADE of 2.64 ± 0.03 eV, which also represents the electron affinity (EA) of the neutral CB_4. A vibrational frequency of 650 ± 80 cm^{-1} is measured for the ground state of neutral CB_4. From the peak position of the A band, the second VDE of CB_4^- is estimated to be ~2.8 eV. The identification of the A band is confirmed in the 266 nm spectrum (Figure 1b), in which the A band is better defined.

(25) Zhai, H. J.; Wang, L. S.; Alexandrova, A. N.; Boldyrev, A. I. *J. Chem. Phys.* **2002**, *117*, 7917.
(26) Wang, L. S.; Cheng, H. S.; Fan, J. *J. Chem. Phys.* **1995**, *102*, 9480.
(27) Becke, A. D. *J. Chem. Phys.* **1993**, *98*, 5648.
(28) Vosko, S. H.; Wilk, L.; Nusair, M. *Can. J. Phys.* **1980**, *58*, 1200.
(29) Lee, C.; Yang, W.; Parr, R. G. *Phys. Rev. B* **1988**, *37*, 785.
(30) (a) Binkley, J. S.; Pople, J. A.; Hehre, W. J. *J. Am. Chem. Soc.* **1980**, *102*, 939. (b) Gordon, M. S.; Binkley, J. S.; Pople, J. A.; Pietro, W. J.; Hehre, W. J. *J. Am. Chem. Soc.* **1982**, *104*, 2797. (c) Pietro, W. J.; Francl, M. M.; Hehre, W. J.; Defrees, D. J.; Pople, J. A.; Binkley, J. S. *J. Am. Chem. Soc.* **1982**, *104*, 5039.
(31) Clark, T.; Chandrasekhar, J.; Spitznagel, G. W.; Schleyer, P. v. R. *J. Comput. Chem.* **1983**, *4*, 294.
(32) Cizek, J. *Adv. Chem. Phys.* **1969**, *14*, 35.
(33) Knowles, P. J.; Hampel, C.; Werner, H.-J. *J. Chem. Phys.* **1993**, *99*, 5219.
(34) Raghavachari, K.; Trucks, G. W.; Pople, J. A.; Head-Gordon, M. *Chem. Phys. Lett.* **1989**, *157*, 479.
(35) (a) Woon, D. E.; Dunning, T. H., Jr. *J. Chem. Phys.* **1993**, *98*, 1358. (b) Kendall, R. A.; Dunning, T. H., Jr.; Harrison, R. J. *J. Chem. Phys.* **1992**, *96*, 6796.
(36) Cederbaum, L. S. *J. Phys. B* **1975**, *8*, 290.
(37) (a) Ortiz, J. V. *Int. J. Quantum Chem., Quantum Chem. Symp.* **1989**, *23*, 321. (b) Lin, J. S.; Ortiz, J. V. *Chem. Phys. Lett.* **1990**, *171*, 197.
(38) Zakrzewski, V. G.; Ortiz, J. V.; Nichols, J. A.; Heryadi, D.; Yeager, D. L.; Golab, J. T. *Int. J. Quantum Chem.* **1996**, *60*, 29.
(39) Bauernshmitt, R.; Alrichs, R. *Chem. Phys. Lett.* **1996**, *256*, 454.
(40) Casida, M. E.; Jamorski, C.; Casida, K. C.; Salahub, D. R. *J. Chem. Phys.* **1998**, *108*, 4439.
(41) Frisch, M. J.; et al. *Gaussian 03*, Revision D.01; Gaussian, Inc.: Wallingford, CT, 2004.
(42) Werner, H.-J.; et al. *MOLPRO*, version 2006.1; see http://www.molpro.net.
(43) Schaftenaar, G. *MOLDEN3.4*; MOLDEN3.4, CAOS/CAMM Center, The Netherlands, 1998.

Table 1. Comparison of the Experimental and Theoretical VDEs of CB_4^- (All Energies Are in eV)

feature	VDE (exp)[a]	final state and electronic configuration	VDE (theor) TD-B3LYP[b]	VDE (theor) ΔRCCSD(T)[c]
		I, CB_4^- (C_s, $^2A''$)		
X[d]	2.64 (3)	$^3A''$, $4a'^2 1a''^2 5a'^2 6a'^2 7a'^1 2a''^1$	2.67	2.84
A	2.8 (1)	$^1A'$, $4a'^2 1a''^2 5a'^2 6a'^2 7a'^2 2a''^0$	2.72	2.65
B	~3.4	$^1A''$, $4a'^2 1a''^2 5a'^2 6a'^2 7a'^1 2a''^1$	3.40	*e*
C	4.34 (3)	$^3A''$, $4a'^2 1a''^2 5a'^2 6a'^1 7a'^2 2a''^1$	4.68	*e*
D	~5.0	$^1A''$, $4a'^2 1a''^2 5a'^2 6a'^1 7a'^2 2a''^1$	5.10	*e*
E	~5.5	$^3A''$, $4a'^2 1a''^2 5a'^1 6a'^2 7a'^2 2a''^1$	5.23	*e*
		$^3A'$, $4a'^2 1a''^1 5a'^2 6a'^2 7a'^2 2a''^1$	5.52	5.39
		II, CB_4^- (C_1, ^2A)		
		^3A, $4a^2 5a^2 6a^2 7a^2 8a^1 9a^1$	2.31	2.52
		^1A, $4a^2 5a^2 6a^2 7a^2 8a^2 9a^0$	2.59	2.22
		^1A, $4a^2 5a^2 6a^2 7a^2 8a^1 9a^1$	3.18	*e*
		^3A, $4a^2 5a^2 6a^2 7a^1 8a^2 9a^1$	4.61	*e*
		^1A, $4a^2 5a^2 6a^2 7a^1 8a^2 9a^1$	5.05	*e*
		^3A, $4a^2 5a^2 6a^1 7a^2 8a^2 9a^1$	5.24	*e*
		^1A, $4a^2 5a^2 6a^1 7a^2 8a^2 9a^1$	5.56	*e*

[a] Numbers in parentheses represent the uncertainty in the last digit. [b] VDEs were calculated at the TD-B3LYP/6-311+G(2df)//B3LYP/6-311+G* level of theory. [c] VDEs were calculated at the RCCSD(T)/6-311+G(2df)//B3LYP/6-311+G* level of theory. [d] A vibrational frequency of 650 ± 80 cm^{-1} is observed. Experimental ADE obtained for CB_4^- is 2.64 ± 0.03 eV. [e] VDEs for those states cannot be calculated at this level of theory.

As will be shown below, the A band is borne out in the theoretical calculations. At 266 nm, another band C is observed at 4.34 eV following a large energy gap. In addition, a weak feature B is barely discernible at ~3.4 eV. As will be shown below, our theoretical results suggest that it is due to a real electronic transition. At 193 nm (Figure 1c), the band B is also weak in intensity, and two more transitions (D, E) are observed at ~5.0 and ~5.5 eV, respectively. The D and E bands are rather broad, suggesting that they may contain vibrational structures or multiple electronic transitions. Note that a weak feature (*) is observed at the low binding energy side in all three spectra. It can be due to either a minor isomer or impurities in the cluster beam. It is unlikely due to a vibrational hot band because of the large excitation energy of this feature relative to the 0−0 transition and our use of the long extension tube to the nozzle, which has been shown to produce relatively cold anions.[11] In addition, in the 266 and 193 nm spectra, some weak signals are observed in the gap between the B and C bands, which may be associated with the same species that gives rise to the low binding energy signal (*). The measured ADE and VDEs of CB_4^- are summarized in Table 1 and compared with the theoretical data, as will be discussed below.

4.2. Photoelectron Spectra of $C_2B_3^-$. Figure 2 shows the photoelectron spectra of $C_2B_3^-$ at 355 and 193 nm. At 355 nm (Figure 2a), a short vibrational progression is resolved for the ground state transition. The intensity of the third vibrational peak is again abnormal due to the low-energy cutoff effect in this case, which is also observed in the 355 nm spectrum of CB_4^- (Figure 1a). The ADE of $C_2B_3^-$ is determined from the intense 0−0 vibrational peak of the X band to be 2.90 ± 0.03 eV. The vibrational progression resolved in the X band of $C_2B_3^-$ yields a frequency of 730 ± 80 cm^{-1}. At 193 nm (Figure 2b), three additional bands (A, B, C) are observed for $C_2B_3^-$. Band A with a VDE of 3.53 eV is broad, indicating unresolved vibrational structures or multiple electronic transitions. Band B at 4.73 eV is relatively sharp and intense, whereas band C at ~6 eV is barely discernible due to poor signal/noise ratios. The low binding energy feature (*) observed in Figure 2 again

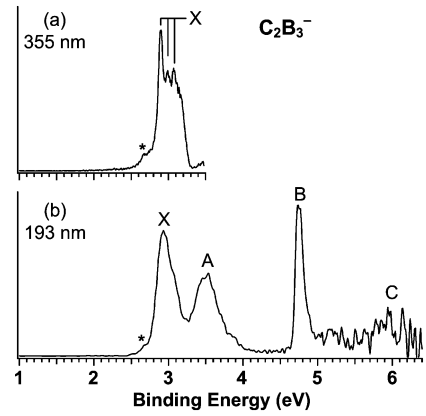

Figure 2. Photoelectron spectra of $C_2B_3^-$ at (a) 355 and (b) 193 nm.

Table 2. Comparison of the Experimental and Theoretical Vertical Detachment Energies (VDE) of $C_2B_3^-$ IV (C_{2v}, $^1A_1$) (All Energies Are in eV)

feature	VDE (exp)[a]	final state and electronic configuration	VDE (theor) TD-B3LYP[b]	VDE (theor) OVGF[c]	VDE (theor) ΔRCCSD(T)[d]
X[e]	2.90 (3)	$^2A_2$, $3a_1^2 2b_2^2 1b_1^2 4a_1^2 3b_2^2 1a_2^1$	2.79	2.88 (0.89)	2.94
A	3.53 (5)	$^2B_2$, $3a_1^2 2b_2^2 1b_1^2 4a_1^2 3b_2^1 1a_2^2$	3.55	3.53 (0.86)	3.50
B	4.73 (3)	$^2A_1$, $3a_1^2 2b_2^2 1b_1^2 4a_1^1 3b_2^2 1a_2^2$	5.02	4.98 (0.86)	4.87
C	~6.0	$^2B_1$, $3a_1^2 2b_2^2 1b_1^1 4a_1^2 3b_2^2 1a_2^2$	5.94	6.08 (0.86)	6.02

[a] Numbers in parentheses represent the uncertainty in the last digit. [b] VDEs were calculated at the TD-B3LYP/6-311+G(2df)//B3LYP/6-311+G* level of theory. [c] VDEs were calculated at the ROVGF/6-311+G(2df)//RCCSD(T)/6-311+G* level of theory. Values in parentheses represent the pole strength of the OVGF calculation. [d] VDEs were calculated at the RCCSD(T)/6-311+G(2df)//RCCSD(T)/6-311+G* level of theory. [e] A vibrational frequency of 730 ± 80 cm^{-1} is resolved. Experimental ADE obtained for $C_2B_3^-$ is 2.90 ± 0.03 eV.

suggests possible contributions from minor isomers or impurities in the cluster beam. The experimental VDEs of $C_2B_3^-$ are presented in Table 2 to be compared with the calculated values.

4.3. Photoelectron Spectra of $C_3B_2^-$, C_4B^-, and C_5^-. The PES spectra of $C_3B_2^-$, C_4B^-, and C_5^- at 193 nm are presented together in Figure 3. One can immediately see a difference between the spectra of these C-rich clusters and those of the B-rich clusters CB_4^- and $C_2B_3^-$: the spectra of the C-rich clusters are all much sharper, suggesting that these clusters are more rigid with little structural change between their anions and neutrals. Aside from the low binding energy peak (X) in C_5^-, the spectra of the C-rich clusters are quite similar to each other, suggesting that they may have similar linear structures like C_5^-. The binding energies of the C-rich clusters are rather high, also reminiscent of the linear carbon clusters, which all have relatively high EAs.[1] For example, the EAs of the linear C_4 and C_6 clusters are 3.882 and 4.185 eV, respectively.[1] The reduced EA of C_5 is a result of its large HOMO−LUMO gap, as defined by the X−A gap observed in the 193 nm spectrum of C_5^- (Figure 3c). Thus, the experimental results already suggest a planar-to-linear structural transition defined by the C or B content in the $C_xB_{5-x}^-$ clusters: the B-rich clusters are likely to be planar, and the C-rich clusters are linear. As will be seen below, these observations are borne out by the theoretical results.

In the 193 nm spectrum of $C_3B_2^-$ (Figure 3a), a total of five well-resolved detachment transitions (X, A−D) are observed. The strong X band defines a VDE of 4.32 eV for the ground state transition. Since no vibrational structure is resolved, the ADE of $C_3B_2^-$ is evaluated from the relatively sharp onset of band X to be 4.21 ± 0.05 eV. Neutral C_3B_2 possesses an even

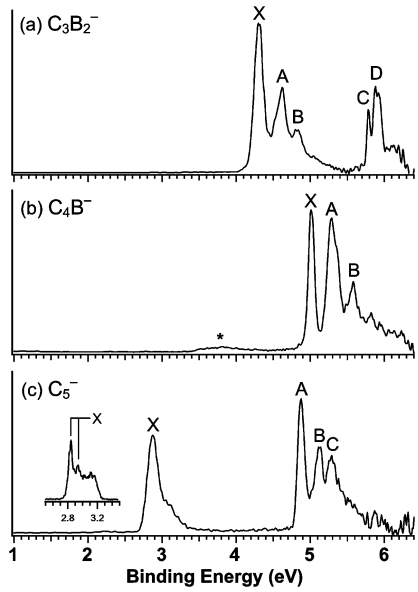

Figure 3. Photoelectron spectra of (a) $C_3B_2^-$, (b) C_4B^-, and (c) C_5^- at 193 nm. The inset in c shows the 355 nm spectrum of C_5^-.

Table 3. Comparison of the Experimental and Theoretical Vertical Detachment Energies (VDE) of $C_3B_2^-$ VI ($C_{\infty v}$, $^2\Sigma^+$) (All Energies Are in eV)

			VDE (theor)	
feature	VDE (exp)[a]	final state and electronic configuration	TD-B3LYP[b]	ΔRCCSD(T)[c]
X[d]	4.32 (3)	$^3\Pi$, $3\sigma^2 4\sigma^2 1\pi^4 5\sigma^2 2\pi^3 6\sigma^1$	4.19	4.39
A	4.62 (4)	$^3\Sigma^+$, $3\sigma^2 4\sigma^2 1\pi^4 5\sigma^1 2\pi^4 6\sigma^1$	4.38	4.45
B	4.83 (4)	$^1\Pi$, $3\sigma^2 4\sigma^2 1\pi^4 5\sigma^2 2\pi^3 6\sigma^1$	5.13	*e*
C	5.79 (3)	$^3\Pi$, $3\sigma^2 4\sigma^2 1\pi^3 5\sigma^2 2\pi^4 6\sigma^1$	5.84	*e*
D	5.90 (4)	$^1\Sigma^+$, $3\sigma^2 4\sigma^2 1\pi^4 5\sigma^2 2\pi^4 6\sigma^0$	5.90	5.93

[a] Numbers in parentheses represent the uncertainty in the last digit. [b] VDEs were calculated at the TD-B3LYP/6-311+G(2df)//B3LYP/6-311+G* level of theory. [c] VDEs were calculated at the RCCSD(T)/6-311+G(2df)//B3LYP/6-311+G* level of theory. [d] Experimental ADE obtained for $C_3B_2^-$ is 4.21 ± 0.05 eV. [e] VDEs for those states cannot be calculated at this level of theory.

number of valence electrons. If C_3B_2 were closed shell, the extra electron in $C_3B_2^-$ should occupy the LUMO, yielding a weak ground state peak followed by a HOMO−LUMO energy gap. The spectral pattern of $C_3B_2^-$—the high electron binding energies, the intense X band, and the lack of an energy gap—suggests that neutral C_3B_2 must be open shell, most likely with a triplet ground state. This observation is also borne out in the theoretical calculations, as seen in Table 3, where the experimental VDEs are compared with the theoretical results.

Only three intense peaks are observed in the spectrum of C_4B^- (Figure 3b). The spectral pattern displays some resemblance to the first three bands in the spectrum of $C_3B_2^-$ but at higher binding energies. The X band of C_4B^- is intense and sharp, yielding an ADE and VDE of 4.99 ± 0.04 and 5.01 ± 0.03 eV, respectively. Some broad and very weak signals are observed at the low binding energy region (*), which again suggests the presence of either minor isomers or impurities in the cluster beam. Weak and unresolved signals are also observed in the high binding energy side beyond 5.7 eV (Figure 3b). These signals could be associated with the weak low binding energy features. The VDEs of C_4B^- are compared with theoretical data in Table 4.

The PES spectra of C_5^- have been reported previously by a number of groups at different photon energies.[44,45] We remeasured the spectra of C_5^- for comparison with those of the B-containing clusters. Our spectra agree with the previously reported data. The 193 nm spectrum of C_5^- is consistent with a closed-shell neutral C_5, which possesses a large HOMO−LUMO gap defined by the X−A separation of 2.04 eV (Figure 3c). The vibrationally resolved 355 nm spectrum of C_5^- yields an ADE of 2.84 ± 0.03 eV (Table 5) and a vibrational frequency of 770 ± 80 cm^{-1}, which agree with those reported by Neumark and co-workers.[45] Despite the fact that the PES of C_5^- has been reported previously, no excited state information was available from these PES studies either due to the low photon energies used or low spectral resolution. The current 193 nm data provide valuable information about the triplet excited electronic states for neutral C_5 (Table 5), as defined by the well-resolved A, B, and C bands (Figure 3c) and discussed later.

5. Theoretical Results and Interpretation of the Photoelectron Spectra of $C_xB_{5-x}^-$ ($x = 1-5$)

The lowest energy structures and a few low-lying isomers obtained from our calculations for $C_xB_{5-x}^-$ ($x = 1-5$) are presented in Figure 4. The planar "W"-shaped (C_{2v}) global minimum structure and chemical bonding of B_5^-, the first member of this series, have been well understood using the B_5^+ cation, which possesses a planar and highly symmetric pentagonal D_{5h} structure. The B_5^+ cluster is shown to exhibit double aromaticity (σ and π) with an electron configuration of $1a_1'^2 1e_1'^4 1e_2'^4 1a_2''^2 2a_1'^2 2e_1'^0$. The first five valence MOs ($1a_1'^2 1e_1'^4 1e_2'^4$) are responsible for the formation of the five two-center two-electron σ B−B peripheral bonds for the cyclic B_5^+. The completely delocalized $1a_2''$ π-MO is responsible for π-aromaticity, and the completely delocalized $2a_1'$ σ-MO is responsible for the σ-aromaticity of B_5^+.[2] Addition of a pair of electrons to the doubly degenerate $2e_1'$ σ-MO results in conflicting aromaticity in the B_5^- anion (π aromatic and σ antiaromatic), and the pentagonal structure is distorted to the "W" shape due to the Jahn−Teller effect. The σ-antiaromaticity is consistent with the relatively low vertical electron detachment energy (VDE), 2.40 ± 0.02 eV, and adiabatic detachment energy (ADE), 2.33 ± 0.02 eV, of B_5^-.[25]

5.1. CB_4^-. The CB_4^- anion has been studied by Pei and Zeng[13] using the basin-hopping algorithm at the DFT (PBE exchange-correlation functional) level of theory with all-electron d-polarization functions including double-numerical basis set. Low-lying isomers were then reoptimized at the B3LYP/6-311+G* level of theory. Single-point calculations of the lowest-energy isomers were also performed at the UCCSD(T)/6-311+G* level. According to Pei and Zeng, at the B3LYP/6-311+G* level of theory, **I** (Figure 4) is the global minimum with **II** being the second lowest isomer 8.1 kcal/mol higher in energy. However, at the UCCSD(T)/6-311+G*//B3LYP/6-311+G* level of theory, they found that **II** is more stable than **I** by 7.0 kcal/mol. Both **I** and **II** are similar to the W-shaped C_{2v} global minimum of B_5^-, ^1A.

(44) (a) Yang, S.; Taylor, K. J.; Craycraft, M. J.; Conceicao, J.; Pettiette, C. L.; Cheshnovsky, O.; Smalley, R. E. *Chem. Phys. Lett.* **1988**, *144*, 431. (b) Handschuh, H.; Gantefor, G.; Kessler, B.; Bechthold, P. S.; Eberhardt, W. *Phys. Rev. Lett.* **1995**, *74*, 1095. (c) Kohno, M.; Suzuki, S.; Shiromaru, H.; Achiba, Y. *J. Chem. Phys.* **1999**, *110*, 3781.

(45) (a) Arnold, D. W.; Bradforth, S. E.; Kitsopoulos, T. N.; Neumark, D. M. *J. Chem. Phys.* **1991**, *95*, 8753. (b) Kitsopoulos, T. N.; Chick, C. J.; Zhao, Y.; Neumark, D. M. *J. Chem. Phys.* **1991**, *95*, 5479.

Table 4. Comparison of the Experimental and Theoretical Vertical Detachment Energies (VDE) of C_4B^- VIII ($D_{\infty h}$, $^1\Sigma_g^+$) (All Energies Are in eV)

			VDE (theor)[b]			
feature	VDE (exp)[a]	final state and electronic configuration	ΔB3LYP	OVGF[c]	RCCSD(T)	CAS-MRCI[d]
X[e]	5.01 (3)	$^2\Pi_g$, $1\pi_u^4 3\sigma_g^2 3\sigma_u^2 1\pi_g^3$	5.25	5.36 (0.88)	5.34 5.39[f] 5.43[g]	4.95
A	5.29 (3)	$^2\Sigma_u^+$, $1\pi_u^4 3\sigma_g^2 3\sigma_u^1 1\pi_g^4$	5.35	5.53 (0.84)	5.24 5.29[f] 5.34[g]	5.12
B	5.58 (4)	$^2\Sigma_g^+$, $1\pi_u^4 3\sigma_g^1 3\sigma_u^2 1\pi_g^4$	5.44	6.66 (0.84)	5.37 5.42[f] 5.46[g]	5.21
		$^2\Pi_u$, $1\pi_u^3 3\sigma_g^2 3\sigma_u^2 1\pi_g^4$	6.79	6.75 (0.86)	6.72 6.76[f] 6.80[g]	6.29

[a] Numbers in parentheses represent the uncertainty in the last digit. [b] Using the 6-311+G(2df) basis set. [c] Values in parentheses represent the pole strength of the OVGF calculation. [d] Calculated as the difference in energy for the anion at CAS(12,10)-MRCISD/6-311+G(2df)//RCCSD(T)/6-311+G* and energy for neutral at CAS(11,10)-MRCISD/6-311+G(2df)//RCCSD(T)/6-311+G*. [e] Experimental ADE obtained for C_4B^- is 4.99 ± 0.04 eV. [f] VDEs were calculated at the RCCSD(T)/aug-cc-pvTZ//RCCSD(T)/6-311+G* level of theory. [g] VDEs were calculated at the RCCSD(T)/aug-cc-pvQZ//RCCSD(T)/6-311+G* level of theory.

Table 5. Comparison of the Experimental and Theoretical Vertical Detachment Energies (VDE) of C_5^- ($D_{\infty h}$, $^2\Pi_u$) (All Energies Are in eV)

			VDE (theor)		
feature	VDE (exp)[a]	final state and electronic configuration	TD-B3LYP[b]	ΔCCSD(T)[c]	ΔCCSDT[d]
X[e]	2.84 (3)	$^1\Sigma_g^+$, $2\sigma_u^2 1\pi_u^4 3\sigma_g^2 3\sigma_u^2 1\pi_g^4 2\pi_u^0$	2.97	2.78	2.81
A	4.88 (4)	$^3\Sigma_u^-$, $2\sigma_u^2 1\pi_u^4 3\sigma_g^2 3\sigma_u^2 1\pi_g^3 2\pi_u^1$	5.09	5.16	5.20
B	5.13 (4)	$^3\Pi_g$, $2\sigma_u^2 1\pi_u^4 3\sigma_g^2 3\sigma_u^1 1\pi_g^4 2\pi_u^1$	5.24	5.06	5.11
C	5.29 (4)	$^3\Pi_u$, $2\sigma_u^2 1\pi_u^4 3\sigma_g^1 3\sigma_u^2 1\pi_g^4 2\pi_u^1$	5.33	5.22	5.25

[a] Numbers in parentheses represent the uncertainty in the last digit. [b] VDEs were calculated at the TD-DFT/6-311+G(2df)//B3LYP/6-311+G* level of theory. [c] VDEs were calculated at the RCCSD(T)/aug-cc-pvTZ//B3LYP/6-311+G* level of theory. [d] VDEs were calculated at the RCCSDT/aug-cc-pvTZ//B3LYP/6-311+G* level of theory. [e] Experimental ADE obtained for C_5^- is 2.84 ± 0.03 eV.

In the current study, we obtained similar results for CB_4^- at the B3LYP/6-311+G* level of theory. According to our calculations, the planar structure **I** is of C_s ($^2A''$) symmetry (Figure 4), which is 8.8 kcal/mol lower in energy than **II** (C_1, ^2A) in complete agreement with the result by Pei and Zeng. However, our UCCSD(T)/6-311+G*//B3LYP/6-311+G* calculations revealed that **I** is more stable than **II** by 2.7 kcal/mol, in disagreement with the result by Pei and Zeng. In order to resolve this discrepancy, we repeated the UCCSD(T)/6-311+G*//B3LYP/6-311+G* calculations using the geometry of Pei and Zeng. With their B3LYP/6-311+G* geometry we obtained the same total energy as reported by Pei and Zeng. The difference between the B3LYP/6-311+G* geometries from the two groups is rather small, and thus, it was puzzling why we had such different UCCSD(T)/6-311+G* results. Analysis of the NORM(A) revealed that in our calculations this value was 1.36, while in the Pei and Zeng calculations it was 1.98. We also noticed very high spin contamination $\langle S^2 \rangle = 1.70$ in our UCCSD(T)/6-311+G* calculation for structure **I**. Thus, UCCSD(T)/6-311+G* calculations for both structures **I** and **II** are not reliable.

In order to resolve the issue on the most stable structure for the CB_4^- cluster, we carried out CASSCF(9,9)-MRCISD/6-311+G*/B3LYP/6-311+G* and CASSCF(9,10)-MRCISD/6-311 +G*/B3LYP/6-311+G* calculations (with 9 active electrons and 9 active orbitals and 9 active electrons and 10 active orbitals, respectively) for **I** and **II**. We found that at this level of theory **I** is lower than **II** by 5.4 kcal/mol (CASSCF(9,9)-MRCISD/6-311+G*) and 1.7 kcal/mol (CASSCF(9,10)-MRCISD/6-311+G*). Thus, according to our CASSCF-MRCISD calculations, structure **I** is the global minimum. However, taking into account the fact that the energy difference between **I** and **II** is only 1.7 kcal/mol at the highest level of theory, we can only tentatively conclude that the global minimum of CB_4^- is structure **I**. In any case, the structural differences between **I** and **II** are rather small, and it is not surprising that they should be fairly close in energy. Because of the high spin contamination for structure **I** we will use the B3LYP/6-311+G* geometry. At this level of theory we do not have any problems with spin contamination. Surprisingly, we found that the optimized geometric parameters for **I** are very similar at the UCCSD(T)/6-311+G* and UCCSD(T)/aug-cc-pvDZ levels of theory to

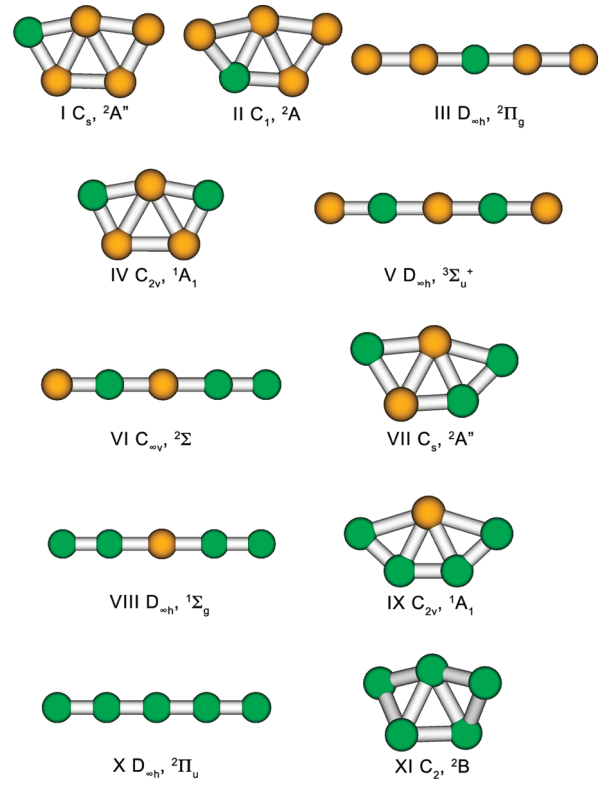

Figure 4. Optimized global minimum and low-lying isomers for CB_4^- (**I**−**III**), $C_2B_3^-$ (**IV** and **V**), $C_3B_2^-$ (**VI** and **VII**), C_4B^- (**VIII** and **IX**), and C_5^- (**X** and **XI**).

those at B3LYP/6-311G* and B3LYP/aug-cc-pvDZ, respectively (Table 1S, Supporting Information).

We also considered linear structures for CB_4^- and found that even the lowest linear structure ($BBCBB^-$) (**III** in Figure 4) is still very high in energy by 51.0 kcal/mol at B3LYP/6-311+G(2df)//B3LYP/6-311+G* and 55.6 kcal/mol at UCCSD(T)/6-311+G(2df)//UCCSD(T)/6-311+G* above the global minimum **I**.

In Table 1 we compare the experimental VDEs with the calculated values for the global minimum **I**, as well as **II** of CB_4^-. We did not calculate VDEs at the UOVGF/6-311+G(2df) level of theory for structures **I** and **II** due to appreciable spin contamination at UHF. We find that **I** agrees better with the experiment and thus will only attempt to interpret the main photoelectron features using this structure. Isomer **II** gives a lower first VDE and may be responsible for the weak low binding energy feature in the PES spectra (Figure 1).

According to our calculations, the two lowest VDEs correspond to electron detachment transitions to the final singlet and triplet states that are very close in energy. The lowest VDE (2.65 eV) obtained at RCCSD(T)/6-311+G(2df)/B3LYP/6-311+G* corresponds to detachment transition to the singlet $^1A'$ final state with an electron configuration of $1a'^2 2a'^2 3a'^2 4a'^2 1a''^2 5a'^2 6a'^2 7a'^2 2a''^0$, which agrees well with the experimental value of 2.64 eV. The second VDE calculated at RCCSD(T)/6-311+G(2df)/B3LYP/6-311+G* (2.84 eV) corresponds to the triplet $^3A''$ final state with an electron configuration of $1a'^2 2a'^2 3a'^2 4a'^2 1a''^2 5a'^2 6a'^2 7a'^1 2a'^1$, also in good agreement with the experimental VDE (2.8 eV). The VDEs calculated at the UCCSD(T)/6-311+G(2df)/B3LYP/6-311+G* level of theory are 2.58 eV ($^1A'$ final state) and 2.63 eV ($^3A''$ final state) and are not reliable since the open-shell states have high spin contamination. The PES pattern (Figure 1) suggests that the ground state of CB_4 is likely open shell with a triplet state, which is in agreement with the TD-DFT calculations (Table 1). If CB_4 were closed shell, the extra electron would occupy its LUMO in the anion, resulting in a weaker PES feature on the low binding energy side and a clear HOMO−LUMO gap, such as that observed for C_5^- (Figure 3c). The triplet ground state of CB_4 is probably the cause for the spin-contamination problems mentioned above. Hence, the TD-DFT energy ordering might be more reliable in this case and is used to assign the CB_4^- spectra.

The weak peak B can be assigned to the transition into the final state $^1A''$ ($1a'^2 2a'^2 3a'^2 4a'^2 1a''^2 5a'^2 6a'^2 7a'^1 2a''^1$). TD-DFT gives a VDE of 3.40 eV for this channel, consistent with the experimental feature B at ~3.4 eV. The fourth peak C with high intensity is assigned to the transition into the final state $^3A''$ ($1a'^2 2a'^2 3a'^2 4a'^2 1a''^2 5a'^2 6a'^1 7a'^2 2a''^1$). The VDE calculated at the TD-DFT level (4.68 eV) for this channel is in reasonable agreement with the experimental value of 4.34 eV. The broad features D and E are tentatively assigned, as shown in Table 1. Overall, the experimental and theoretical data agree reasonably well for isomer **I**, providing credence for the C_s planar structure as the global minimum for CB_4^- with isomer **II** as a low-lying isomer. The corresponding ground states of the neutral CB_4 for both structures are triplet states give rise to the complicated PES spectra as shown in Figure 1.

Since the optimized geometries of the neutral singlet and triplet states are similar to the geometry of the anionic doublet state, only vibrational modes with the a′ symmetry are expected to be active during photodetachment transitions. For the singlet state, there are three a′ modes with frequencies of $\omega_3(a') = 529$ cm^{-1}, $\omega_4(a') = 706$ cm^{-1}, and $\omega_5(a') = 778$ cm^{-1} at the B3LYP/6-311+G* level of theory. For the triplet state there are also three a′ modes with frequencies of $\omega_3(a') = 463$ cm^{-1}, $\omega_4(a') = 628$ cm^{-1}, and $\omega_5(a') = 775$ cm^{-1} at the same level of theory. Thus, the $\omega_4(a') = 628$ cm^{-1} vibrational mode of the triplet state is in good agreement with the observed vibrational progression of 650 cm^{-1}, providing additional evidence for the global minimum of CB_4^- and the triplet nature of the CB_4 ground state.

5.2. $C_2B_3^-$. The $C_2B_3^-$ cluster has not been studied before. We find that the global minimum of $C_2B_3^-$ is a planar C_{2v} ($^1A_1$) structure (**IV** in Figure 4) at the B3LYP/6-311+G* level of theory. This structure is similar to the global minimum of CB_4^- discussed above and the W-shaped structure of B_5^-, ^1A. The optimized structural parameters for **IV** are very similar at the RCCSD(T)/6-311+G* and RCCSD(T)/aug-cc-pvDZ levels of theory (Table 2S, Supporting Information). The lowest linear isomer **V** has a $BCBCB^-$ atomic arrangement (**V** in Figure 4), which is higher in energy than **IV** by 12.2 kcal/mol at B3LYP/6-311+G(2df)//B3LYP/6-311+G* and 22.7 kcal/mol at RCCSD(T)/6-311+G(2df)//CCSD(T)/6-311+G*.

Experimental and theoretical VDEs for the global minimum **IV** are compared in Table 2. The first VDE calculated at the three levels of theory, 2.79 eV [B3LYP/6-311+G(2df)//B3LYP/6-311+G*], 2.88 eV [OVGF/6-311+G(2df)//RCCSD(T)/6-311+G*], and 2.94 eV [RCCSD(T)/6-311+G(2df)//RCCSD(T)/6-311+G*], are consistent with each other, all agreeing well with the experimental value of 2.90 eV. It corresponds to electron detachment from the $1a_2$ HOMO, which leads to the doublet $^2A_2$ final state with an electron configuration of $1a_1^2 1b_2^2 2a_1^2 3a_1^2 2b_2^2\ 1b_1^2 4a_1^2 3b_2^2 1a_2^1$. Since the optimized geometry of the neutral doublet state is similar to that of the anionic singlet state, only vibrational modes with a_1 symmetry are expected to be active. The vibrational frequency observed for the X band (725 ± 80 cm^{-1}) is in good agreement with the lowest calculated frequency (735 cm^{-1}) for a totally symmetric mode (a_1) of C_2B_3 at the B3LYP/6-311+G* level of theory. The second VDE from **IV** calculated at all three levels of theory is again consistent with each other and is in excellent agreement with the experiment (Table 2). The third VDE calculated at the RCCSD(T)/6-311+G(2df)//CCSD(T)/6-311+G* level (4.87 eV) is in good agreement with the experimental value (4.73 eV). However, the B3LYP/6-311+ G(2df) and ROVGF/6-311+G(2df) methods appear to have slightly overestimated this VDE. Finally, the broad and weak feature C at ~6.0 eV observed in the 193 nm spectrum (Figure 2b) is also well reproduced by all three levels of theory (Table 2). The overall agreement between theory and experiment for $C_2B_3^-$ is excellent, confirming unequivocally the C_{2v} global minimum structure **IV** for this cluster.

5.3. $C_3B_2^-$. Our calculations show that the global minimum of $C_3B_2^-$ is a linear structure with the $BCBCC^-$ atomic arrangement (**VI**, Figure 4) and $C_{\infty v}$ symmetry. It possesses a doublet ground state, $^2\Sigma^+$ ($1\sigma^2 2\sigma^2 3\sigma^2 4\sigma^2 1\pi^4 5\sigma^2 2\pi^4 6\sigma^1$). Because of high spin contamination ($\langle S^2\rangle = 1.20$) we did not use the UCCSD(T)/6-311+G* geometry and did not run UOVGF/6-311+G(2df) calculations. Instead, we used the B3LYP/6-311+G* geometry ($\langle S^2\rangle = 0.77$ at this level of theory) for all other high-level calculations. In spite of high spin contamination at the UCCSD(T) level of theory, the optimized bond lengths for **VI** are very similar using UCCSD(T)/6-311+G*, UCCSD(T)/aug-cc-pvDZ, B3LYP/6-311+G*, and B3LYP/aug-cc-pvDZ (Table 3S, Supporting Information). The lowest nonlinear planar isomer (**VII**, C_s, $^2A''$, Figure 4) is higher in energy than the

linear structure **VI** by 27.5 kcal/mol at B3LYP/6-311+G(2df)s//B3LYP/6-311+G* and 22.1 kcal/mol at RCCSD(T)/6-311+G-(2df)//B3LYP/6-311+G*.

In Table 3, we compare the theoretical VDEs with the experimental data for the global minimum **VI** of $C_3B_2^-$. The first VDE corresponds to electron detachment from the 2π orbital resulting in a triplet final state ($^3\Pi$) with a $1\sigma^2 2\sigma^2 3\sigma^2 4\sigma^2 1\pi^4 5\sigma^2 2\pi^3 6\sigma^1$ configuration. This result is consistent with the experimental evidence that the neutral C_3B_2 cluster is not closed shell, as mentioned in section 4.3. The calculated VDE is 4.19 eV at B3LYP/6-311+G(2df)//B3LYP/6-311+G* and 4.39 eV at RCCSD(T)/6-311+G(2df)//B3LYP/6-311+G*, both in good agreement with the experimental value of 4.32 eV. The second peak A is due to the transition into the final state $^3\Sigma^+$ ($1\sigma^2 2\sigma^2 3\sigma^2 4\sigma^2 1\pi^4 5\sigma^1 2\pi^4 6\sigma^1$). The computed VDEs at B3LYP/6-311+G(2df)//B3LYP/6-311+G* (4.38 eV) and RCCSD(T)/6-311+G(2df)//B3LYP/6-311+G* (4.45 eV) are consistent with each other and agree reasonably well with the experiment (4.62 eV). We were not able to calculate the VDE with the $^1\Pi$ ($1\sigma^2 2\sigma^2 3\sigma^2 4\sigma^2 1\pi^4 5\sigma^2 2\pi^3 6\sigma^1$) final state at the RCCSD(T) level of theory, and our calculated VDE (5.13 eV) at B3LYP/6-311+G(2df)//B3LYP/6-311+G* is somewhat higher than the experimental peak B at 4.83 eV. The features C and D are originated from detachment transitions to the final states $^3\Pi$ ($1\sigma^2 2\sigma^2 3\sigma^2 4\sigma^2 1\pi^3 5\sigma^2 2\pi^4 6\sigma^1$) and $^1\Sigma^+$ ($1\sigma^2 2\sigma^2 3\sigma^2 4\sigma^2 1\pi^4 5\sigma^2 2\pi^4 6\sigma^0$), respectively, according to our B3LYP/6-311+G(2df)//B3LYP/6-311+G* calculations (Table 3). The overall agreement between the calculated VDEs and the PES data is very good, confirming the linear global minimum structure of $C_3B_2^-$.

It should be pointed out that the VDE increases by 1.42 eV from $C_2B_3^-$ (2.90 eV) to $C_3B_2^-$ (4.32 eV). In fact, the VDE of $C_3B_2^-$ is higher than that of Cl^- (3.617 eV)[46] and thus can be called a superhalogen.[47] The high binding energy $C_3B_2^-$ is likely associated with its linear structure, which is consistent with the fact that all small linear carbon clusters have relatively large electron affinities.[1] Thus, both experimental and theoretical evidence suggests that the transition from planar to linear structure occurs at the $C_3B_2^-$ cluster.

5.4. C_4B^-. There have been a few previous theoretical calculations on CB_4^-. A linear CCCCB$^-$ structure was suggested for CB_4^- at the RHF/3-21G level of theory.[5] Subsequent MP2 calculations with various basis sets[15] also gave the linear CCCCB$^-$ singlet structure for CB_4^-. In our B3LYP/6-311+G* structural search we found a linear structure (**VIII**, Figure 4) with a CCBCC$^-$ ($D_{\infty h}$, $^1\Sigma_g^+$) atomic arrangement to be the global minimum. Geometry optimization and frequency calculations at the RCCSD(T)/6-311+G* and RCCSD(T)/aug-cc-pvdz levels of theory confirmed this structure (Table 4S, Supporting Information). The linear singlet CCCCB$^-$ ($C_{\infty v}$, $^-\Sigma^+$) structure as reported previously[5,15] is 28.8 kcal/mol (at B3LYP/6-311+G(2df)//B3LYP/6-311+G*) higher in energy than the global minimum **VIII**. Among nonlinear planar isomers the lowest structure **IX** (C_{2v}, $^1A_1$) is higher than the global minimum **VIII** by 66.2 kcal/mol (B3LYP/6-311+G(2df)//B3LYP/6-311+G*) and 57.5 kcal/mol (RCCSD(T)/6-311+G(2df)//RCCSD(T)/6-311+G*). Clearly, upon further increasing the number of carbon atoms in the $C_xB_{5-x}^-$ series, the planar structures continue to become less favorable in energy than the linear structures. In Table 4, we present the experimental and theoretical VDEs for the global minimum structure **VIII**.

We can see that the overall patterns of the computed VDEs by all four methods are consistent qualitatively with the experimental spectrum (Figure 3b): three lower-lying transitions ($^2\Pi_g$, $^2\Sigma_u^+$, and $^2\Sigma_g^+$) corresponding to the three observed bands followed by a transition to the $^2\Pi_u$ final state, which is beyond the 193 nm photon energy. However, we found that the computational results at four levels of theory show some significant variations. At B3LYP/6-311+G(2df)//B3LYP/6-311+G*, the computed VDEs to the three lowest final states, $^2\Pi_g$, $^2\Sigma_u^+$, and $^2\Sigma_g^+$, are close to each other, while the results at UOVGF/6-311+G(2df)//RCCSD(T)/6-311+G* are overestimated, in particular for the $^2\Sigma_g^+$ final state. At RCCSD(T)/6-311+G(2df) the first three calculated VDEs are almost degenerate with the $^2\Sigma_u^+$ state being the lowest at this level of theory. These results are highly unusual for a relatively small main-group cluster. We usually observe very good agreement between experimental and theoretical VDEs at the CCSD(T)/6-311+G(2df) level of theory if the spin contamination is small. In order to investigate whether the 6-311+G(2df) basis set causes the problem, we performed RCCSD(T) calculations with two extended aug-cc-pvTZ and aug-cc-pvQZ basis sets, as given in Table 4. One can see that calculated VDEs at these two basis sets do not deviate more than 0.1 eV from the results at RCCSD(T)/6-311+G(2df). Thus, the 6-311+G(2df) basis set is not responsible for the poor agreement with experiment. We performed additional VDE calculations using CAS(12,10)-MRCISD/6-311+G(2df)//RCCSD(T)/6-311+G* for the anion and CAS(11,10)-MRCISD/6-311+G(2df)//RCCSD(T)/6-311+G* for the neutral to check for multiconfigurational characters. While the first VDE (4.95 eV) calculated at this level of theory is now in good agreement with the experimental value (5.01 eV), the second and third VDEs are underestimated. The C_4B^- cluster seems to be a conundrum for computational chemistry at the current levels, and further investigation certainly is needed to achieve better agreement with the experiment.

Nevertheless, the qualitative agreement between the computed VDEs at the different levels of theory and the experimental spectrum provides support for the identified global minimum **VIII**. The CCCCB$^-$ isomer can be safely ruled out as a major contributor to the experimentally observed spectrum because its first VDE (3.78 eV) computed at B3LYP/6-311+G(2df)//B3LYP/6-311+G*) is much lower than the VDE of the X band (5.01 eV). In fact, the CCCCB$^-$ isomer may be the carrier for the weak feature observed at ~3.8 eV (Figure 3b). Another linear singlet isomer CCCBC$^-$ was found to be very high in energy, 64.7 kcal/mol at the B3LYP/6-311+G* level, with respect to the global minimum and can be firmly ruled out as the carrier of C_4B^-.

5.5. C_5^-. The global minimum of C_5^- is well known to be linear with a $^2\Pi_u$ electronic state from previous experimental and theoretical studies.[1,44,45,48−53] The current calculations also find the global minimum linear structure for C_5^- (**X**, Figure 4), consistent with the previous works. The calculated first VDE at all three levels of theory is in good agreement with the experimental data (Table 5). The three higher-lying VDEs (A, B, C) are very close to each other, and we cannot assign them with certainty. We present the tentative assignments for these

(46) Hotop, H.; Lineberger, W. C. *J. Phys. Chem. Ref. Data* **1985**, *14*, 731.
(47) Gutsev, G. L.; Boldyrev, A. I. *Chem. Phys.* **1981**, *56*, 277.
(48) (a) Adamowicz, L. *Chem. Phys. Lett.* **1991**, *180*, 466. (b) Watts, J. D.; Bartlett, R. J. *J. Chem. Phys.* **1992**, *97*, 3445.
(49) Ohara, M.; Shiromaru, H.; Achiba, Y.; Aoki, K.; Hashimoto, K.; Ikuta, S. *J. Chem. Phys.* **1995**, *103*, 10393.

three bands in Table 5 according to the TD-B3LYP results, which seem to be in better agreement with the experiment. In addition, we also calculated a quasi-planar structure for C_5^- (C_2, ^2B), as shown in Figure 4 (**XI**). This structure is much higher in energy than the linear structure **X** by 85.3 kcal/mol at B3LYP/6-311+G(2df)//B3LYP/6-311+G* and 70.7 kcal/mol at UCCSD(T)/6-311+G(2df)//B3LYP/6-311+G*.

The spectroscopy of neutral C_5 has been studied extensively because of its importance in astrophysics.[54] A number of electronic excited states have been calculated and experimentally detected.[55] However, from the singlet ground state ($^1\Sigma_g^+$) of C_5 only singlet excited states have been observed and considered. As shown in Table 5, the observed excited states in the current experiment (A, B, C) all correspond to triplet excited states, which are not known before. Even though the resolution of the current PES spectrum at 193 nm is limited, the excitation energies for these triplet excited states can be estimated from the VDE differences relative to the ground state X and should be valuable to compare to future computational studies aimed at understanding the low-lying excited state manifold of C_5.

6. Structural Transitions and Chemical Bonding in the $C_xB_{5-x}^-$ ($x = 1-5$) Clusters

The structural transition in the $C_xB_{5-x}^-$ clusters can be understood from the chemical bonding of the cyclic and linear structures. Both natural bond analysis (NBO)[56] and the adaptive natural density partitioning method (AdNDP)[57] are used for the bonding analyses. The NBO method gives rise to lone pairs and two-center two-electron (2c-2e) bonds, while the AdNDP method can reveal multicenter (*n*c-2e) bonds. These analyses were performed at the B3LYP/6-311+G* level of theory.

In order to understand the planar structures of the B-rich $C_xB_{5-x}^-$ clusters, we start our analysis with the B_5^+ cluster, which was shown previously to possess a slightly distorted pentagonal structure.[58] However, if zero-point energy corrections are taken into account the vibrationally averaged structure of B_5^+ is a perfect pentagon,[2] whose bonding has been explained through the formation of five 2c-2e peripheral σ B−B bonds and double σ- and π-aromaticity by AdNDP.[2,57a] The double aromaticity in B_5^+ is consistent with the high stability of B_5^+ observed experimentally.[59] The most stable linear B_5^+ structure at the B3LYP/6-311+G* level was found to be a heptet state ($^7\Sigma_u^+$) with the following valence electronic configuration: $1\sigma_g^2 1\sigma_u^2 2\sigma_g^2 2\sigma_u^2\ 3\sigma_g^1 1\pi_u^2 3\sigma_u^1 1\pi_g^2$, which is 78.0 kcal/mol higher in energy than the global minimum pentagonal structure. For the B_5^+ linear structure, our NBO analyses show four 2c-2e σ B−B bonds with occupation numbers (ON) of 2.00 |e|. The six unpaired electrons in the $3\sigma_g^1 1\pi_u^2 3\sigma_u^1 1\pi_g^2$ MOs form a pair of localized electrons with ON = 1.00 |e| each on the terminal atoms and four singly occupied π-bonds (ON = 0.84 |e|) on two pairs of B−B atoms at the two ends of the linear structure. The low occupation numbers on those four π B−B bonds is a sign of the conjugation of these bonds with the central boron atom. The superior bonding pattern in the cyclic pentagon structure (five 2c-2e σ B−B peripheral bonds and double aromaticity characterized by the completely delocalized 5c-2e σ bond and 5c-2e π bond) makes it significantly more stable than the linear isomer (four 2c-2e σ−B-B bonds and four 2c-1e π-bonds).

Upon addition of electrons along the $C_xB_{5-x}^-$ series with increasing x, the linear structures gain additional bonding orders through double occupation of the 2c-1e π-bonds, while the occupation of delocalized σ- and π-MOs in the cyclic structure brings antibonding character. For example, in the linear global minimum structure **VIII** of C_4B^- (Figure 4), the partially occupied $3\sigma_g^1 1\pi_u^2 3\sigma_u^1 1\pi_g^2$ MOs in B_5^+ are now completely occupied, forming the closed-shell electron configuration $1\sigma_g^2 1\sigma_u^2 2\sigma_g^2 2\sigma_u^2 3\sigma_g^2 1\pi_u^4 3\sigma_u^2 1\pi_g^4$, i.e., addition of the six electrons upon going from linear B_5^+ to linear C_4B^- fills up all the partially occupied MOs in B_5^+. NBO analysis for C_4B^- reveals the presence of two lone pairs (ON = 1.96 |e|) on the terminal carbon atoms, two 2c-2e σ-B−C bonds (ON = 1.99 |e|), two 2c-2e σ-C−C bonds (1.99 |e|), and four 2c-2e π-C−C bonds (ON = 1.79 |e|). Thus, from the B_5^+ linear structure to the C_4B^- linear structure one gains a total of two bond orders.

At the same time, going from B_5^+ to B_5^- one looses σ-aromaticity in the cyclic structure, because the number of delocalized σ-electrons is now four.[2,59] However, the B_5^- cluster is still a π-aromatic system. From the cyclic B_5^- to $C_2B_3^-$ the additional two electrons go to the delocalized π-MOs, making the $C_2B_3^+$ cluster a globally doubly σ- and π- antiaromatic system with four delocalized π-electrons and four delocalized σ-electrons. Though the $C_2B_3^-$ cyclic structure is still more stable than the linear one, the difference between these two types of structures, 22.7 kcal/mol at RCCSD(T)/6-311+G(2df), becomes relatively small. Hence, with addition of just one more electron upon going from $C_2B_3^-$ to $C_3B_2^-$ the linear structure becomes more stable. Upon further occupation of MOs in the linear structure going from $C_3B_2^-$ to C_4B^- we reach the point where we have two triple bonds at the two ends of the five-atom cluster and achieve the maximum bond order. The neutral C_5 cluster is isoelectronic to the C_4B^- anion and is known to be an extremely stable species detected both in flames and in interstellar space.[54] The high stability of C_5 is also evidenced by its large HOMO−LUMO gap, which is responsible for the anomalously low EA for C_5 (Figure 3c).

Therefore, the $C_xB_{5-x}^-$ series of clusters provides us a rare opportunity to examine the cyclic to linear transition, atom-by-

(50) Gotts, N. G.; von Helden, G.; Bowers, M. T. *Int. J. Mass Spectrom. Ion Processes* **1995**, *149/150*, 217.
(51) Szczepanski, J.; Ekern, S.; Vala, M. *J. Phys. Chem. A* **1997**, *101*, 1841.
(52) (a) Freivogel, P.; Grutter, M.; Forney, D.; Maier, J. P. *Chem. Phys.* **1997**, *216*, 401. (b) Forney, D.; Grutter, M.; Freivogel, P.; Maier, J. P. *J. Phys. Chem. A* **1997**, *101*, 5292.
(53) Szczepanski, J.; Hodyss, R.; Vala, M. *J. Phys. Chem. A* **1998**, *102*, 8300.
(54) Bernath, P. F.; Hinkle, K. H.; Keady, J. J. *Science* **1989**, *244*, 562.
(55) (a) Boguslavskiy, A. E.; Maier, J. P. *J. Chem. Phys.* **2006**, *125*, 094308. (b) Kolbuszewski, M. *J. Chem. Phys.* **1995**, *102*, 3679. (c) Hanrath, M.; Peyerimhoff, S. D. *Chem. Phys. Lett.* **2001**, *337*, 368.
(56) (a) Foster, J. P.; Weinhold, F. *J. Am. Chem. Soc.* **1980**, *102*, 7211. (b) Reed, A. E.; Curtiss, L. A.; Weinhold, F. *Chem. Rev.* **1988**, *88*, 899. (c) Weinhold, F.; Landis, C. R. *Valency and Bonding: A Natural Bond Orbital Donor-Acceptor Perspective*; Cambridge University Press: Cambridge, U.K., 2005.
(57) (a) Zubarev, D. Yu.; Boldyrev, A. I. *Phys. Chem. Chem. Phys.* **2008**, *10*, 5207. (b) Zubarev, D. Yu.; Boldyrev, A. I. *J. Org. Chem.* **2008**, *73*, 9251. (c) Zubarev, D. Yu.; Boldyrev, A. I. *J. Phys. Chem. A* **2009**, *113*, 866. (d) Zubarev, D. Yu; Robertson, N.; Domin, D.; McClean, J.; Wang, J.; Lester, W. A., Jr.; Whitesides, R.; You, X.; Frenklach, M. *J. Phys. Chem. C* **2010**, *114*, 5429.
(58) (a) Kato, H.; Yamashita, K.; Morokuma, K. *Chem. Phys. Lett.* **1992**, *190*, 361. (b) Ricca, A.; Bauschlicher, C. W., Jr. *Chem. Phys.* **1996**, *208*, 233.
(59) (a) Hanley, L.; Anderson, S. L. *J. Phys. Chem.* **1987**, *91*, 5161. (b) Hanley, L.; Anderson, S. L. *J. Chem. Phys.* **1988**, *89*, 2848. (c) Hanley, L.; Whitten, J. L.; Anderson, S. L. *J. Phys. Chem.* **1988**, *92*, 5803. (d) Hintz, P. A.; Ruatta, S. A.; Anderson, S. L. *J. Chem. Phys.* **1990**, *92*, 292.

atom and electron-by-electron and also allows us to gain further insight into the bonding and stability of the important linear C_5 cluster.

7. Conclusions

We report a photoelectron spectroscopic and theoretical investigation of boron−carbon mixed clusters containing five atoms, $C_xB_{5-x}^-$ ($x = 1-5$). The electron binding energies were observed to increase abruptly from $x = 2$ to 3, signaling a major structural transition. Theoretical calculations at different levels of theory were performed and compared with the experimental results. We observed a planar-to-linear structural transition as a function of x, consistent with the experimental observation. The CB_4^- and $C_2B_3^-$ clusters are found to possess distorted pentagonal planar structures similar to B_5^-, whereas $C_3B_2^-$ and C_4B^- are shown to be linear similar to C_5^-. Our results suggest that in B-rich clusters (CB_4^- and $C_2B_3^-$) the C atoms act as minor dopants replacing one or two B atoms in the planar B_5^- cluster without too much structural distortion. For C-rich clusters ($C_3B_2^-$ and C_4B^-), the B atoms act as minor dopants into the linear structure of C_5^-. We show that the most favorable bonding in the planar structure occurs in the B_5^+ cluster, which possesses five 2c-2e σ-B−B peripheral bonds plus a 5c-2e σ-bond and a 5c-2e π-bond. Along the $C_xB_{5-x}^-$ ($x = 1-5$) series the planar structures become less stable due to the increasing antibonding character in the delocalized σ- and π-bonds, while the linear structures gain stability due to the formation of π-bonds. We show that the linear C_4B^- or C_5 has the most stable electronic configuration and bonding among the linear clusters. It would be interesting to investigate larger B/C mixed clusters to systematically examine the planar-to-linear structure transitions in $C_xB_y^-$ clusters as a function of composition.

Acknowledgment. The experimental work was supported by the National Science Foundation (DMR-0904034 to L.S.W.). The theoretical work was supported by the National Science Foundation (CHE-0714851 to A.I.B). Computer time from the Center for High Performance Computing at Utah State University is gratefully acknowledged. The computational resource, the Uinta cluster supercomputer, was provided through the National Science Foundation under Grant CTS-0321170 with matching funds provided by Utah State University.

Supporting Information Available: Optimized geometry of the lowest isomers of $C_xB_{5-x}^-$ ($x = 1-4$) at CCSD(T)/6-311+G* and CCSD(T)/aug-cc-pvDZ and the complete citation of refs 41 and 42. This material is available free of charge via the Internet at http://pubs.acs.org.

JA103846Q